

Article

A Single-Stage High-Power Factor Converter with Synchronized Self-Excited Technique for LED Lighting

Yong-Nong Chang ¹, Shun-Yu Chan ² and Hung-Liang Cheng ^{3,*} 

¹ Department of Electrical Engineering, National Formosa University, Yunlin County 63201, Taiwan; ynchang@nfu.edu.tw

² Department of Electrical Engineering, Cheng Shiu University, Kaohsiung 83347, Taiwan; gitanojan@gmail.com

³ Department of Electrical Engineering, I-Shou University, Kaohsiung 84001, Taiwan

* Correspondence: hlcheng@isu.edu.tw; Tel.: +886-7-657-7711 (ext. 6634)

Received: 16 July 2018; Accepted: 16 August 2018; Published: 20 August 2018



Abstract: This paper proposes a single-stage, high power-factor light-emitting diode (LED) driver with a self-excited control scheme for the power switches. The self-excited mechanism is accomplished by fetching the driving voltages from a center-tapped transformer. The frequency of the driving voltages is exactly the same as the resonant frequency of the resonant converter, thus synchronizing the resonant frequency with the switching frequency and achieving zero-voltage switching (ZVS) and zero-current switching (ZCS) of power switches. The circuit topology is mainly composed of a half-bridge LC resonant converter, along with a boost-type power-factor corrector (PFC) to fulfill the single-stage structure, meaning that the presented LED driver possesses high power-factor features and low switching loss. Finally, a 40 W prototype circuit is implemented and tested, and the experimental results exhibit a satisfactory performance.

Keywords: light-emitting diode (LED); power-factor correction; self-excited; single stage; soft switching

1. Introduction

Light-emitting diode (LED) lighting has many advantages, such as high lighting efficiency, a compact size, and fast response. When compared with fluorescent lamps, LEDs are more environmentally friendly because they do not use mercury. As such, with these features, the usage of LED lighting has become an irresistible trend. Among the various advantages of LED, the most prominent still focuses on its high lighting efficiency, although not all questions about the interaction between humans and light emitted by the LEDs have been completely solved [1–3]. Nowadays, in pursuit of things such as high lighting quality, special lighting atmospheres, and/or energy-saving capacities, many LED lights have incorporated a dimming function. However, because there are many people who do not require higher-quality lighting, LED lighting without the dimming function is still widely used, such as in household or street lighting. For such lights, the key factor of lighting equipment selection depends on the cost–performance ratio of the product [4–6]. Thus, the development of a simple and low-cost LED driver is likely to greatly enhance the popularity of LED lighting.

In the highly-competitive lighting market, the lighting drive circuit, using a self-excited control mechanism, has been widely used in many low-price products—especially in the applications of electronic ballast [7–10]. The purpose of a self-excited circuit is to drive the power switches repeatedly

by using the polarity changes of the voltage across windings of a magnetic component, meaning that it does not need to use an integrated circuit (IC), and the components used to build a direct-current (dc) voltage for the IC can be saved. In the conventional self-excited fluorescent lamp electronic ballast, the circuit topology possesses a half-bridge (inductor-capacitor-capacitor) (LCC) resonant circuit by introducing a saturable transformer connected in series with a resonant circuit to generate the self-excited driving voltage that can drive bipolar junction transistors (BJT) [11–13]. Regarding driving a BJT, when it is used as a power switch, it requires a base current sufficiently high enough to drive the BJT to operate in the saturation region. However, driving a BJT into the saturation region will influence the charge carrier behavior in the (positive-negative) (PN) junction, thus further affecting the switching time thereof. In general, there are many such uncontrollable factors, including things like saturation point of an iron core, storage time carriers, ambient temperature, and humidity—and all of them hinder the precise control of the resonant frequency and voltage gain of the resonant circuit.

On the other hand, active power-factor correctors (PFCs) are widely applied to the lighting circuit due to the increasingly strict regulations on power quality. Although the power factor can be effectively improved by adding a PFC circuit to the original lighting circuit, the number of circuit components then need to be increased, resulting in an uneconomical solution. Thus, aiming to find a cost-effective solution, researchers proposed some single-stage lighting circuits with self-excited control schemes by integrating a PFC and dc-to-dc resonant circuit [14–16]. However, using BJT as power switches invokes further problems [17], because among these single-stage circuits, two power BJTs could suffer from uneven current and lead to unequal conduction time between the two BJTs, thus making the simplification of single-stage PFC impossible.

In this paper, a novel single-stage LED driver with a self-excited mechanism through integration of a boost-type PFC and a half-bridge series resonant converter is proposed. No additional integrated circuit is required. The driving voltages of the self-excited mechanism are taken directly from the center-tapped transformer, which is cascaded by a full-wave diode rectifier to obtain the dc output voltage. As compared with the traditional self-excited mechanism, it does not need to use an easily saturable transformer—thus, the number of components can be reduced. Two metal-oxide-semiconductor field-effect transistors (MOSFETs) serve as the power switches. The MOSFET is a voltage-driven component. Unlike the BJT-based circuit topology, the core saturation and carrier storage time problems can be avoided, thus making the circuit design easier. Moreover, since MOSFETs are used in the single-stage PFC circuit, the incidence of unequal currents in power switches is far less, meaning the uneven conduction times between the switches can be ignored. Therefore, the developed self-excited method is quite suitable for single-stage PFC application. In addition, the switching frequency of the MOSFETs can be identical to the resonant frequency of the resonant converter. The resonant converter operates at the resistive mode, thus accomplishing both the zero-voltage switching (ZVS) and zero-current switching (ZCS) performance of power switches [18–21]. Consequently, the developed self-excited single-stage converter will possess the advantages of having both a high power factor and low switching losses, and is also suitable for LED drive application.

2. Proposed Circuit Topology and Operation Analysis

In our particular study, a half-bridge inductor-capacitor (LC) resonant converter, a boost-typed PFC, a starter circuit, and the developed self-excited circuit were integrated to constitute the novel single-stage structure, as shown in Figure 1. A list of symbols is as follows.

S_1, S_2 : power switches; D_{S1}, D_{S2} : intrinsic body diodes of the power switches, L_{PFC} : inductance of the boost-typed PFC, T_1 : center-tapped transformer, N_p : turns of the primary winding, N_{S1}, N_{S2} : turns of the secondary windings, N_{SE1}, N_{SE2} : turns of the self-excited windings, D_1, D_2 : full-wave rectifier diodes, L_r : inductance of the resonant inductor, C_r : capacitance of the resonant capacitor, L_m : inductance of the low-pass filter, C_m : capacitance of the low-pass filter, C_{bus} : capacitance of the dc-bus capacitor, and C_o : capacitance of the output capacitor.

v_{in} : input line voltage, i_{in} : input line current, i_{LPFC} : PFC inductor current, V_{cbus} : dc-bus voltage, i_{cbus} : dc-bus current, V_o : output voltage, v_{gs1} : gate-to-source voltage of S_1 , v_{gs2} : gate-to-source voltage of S_2 , i_{S1} : drain-to-source current of S_1 , i_{S2} : drain-to source current of S_2 , i_r : resonant current of the resonant circuit, v_{AB} : input voltage of the resonant circuit, v_p : voltage across the primary winding, f_r : resonant frequency of the resonant circuit, f_s : switching frequency of power switches, M_{vr} : voltage gain of the resonant circuit, Q : quality factor of the resonant circuit, ω_s : switching angular frequency, ω_r : resonant angular frequency, R_p : equivalent load resistance across the primary winding, R_{LED} : equivalent resistance of the LED string, and D : duty ratio of the power switches.

MOSFETs S_1 and S_2 acted as power switches, and the antiparallel diodes D_{S1} and D_{S2} as their intrinsic body diodes, respectively. The center-tapped transformer T_1 and diodes D_1 and D_2 formed a full-wave rectifier. The turn ratio of the primary winding to the secondary windings was n : 1:1. In addition, T_1 had two more windings which were employed to provide power switches with self-excited driving voltages. Besides, T_1 could provide galvanic insulation with respect to the input line. The low-pass filter (L_m and C_m) was used to remove the high-frequency current of the inductor current, because in this way, the input line current would be sinusoidal with the same frequency as the input line voltage. For simplification of the circuit analysis, the capacitances of C_{bus} and C_o were assumed to be large enough that the dc-bus voltage V_{cbus} and the output voltage V_o could be regarded as constant. As shown in Figure 1, the power switch S_2 should carry both currents of the PFC converter and the resonant converter. The voltage across S_2 is equal to the dc-bus voltage when it is off. Hence, S_2 is the crucial component of the proposed circuit and its voltage and current ratings will determine the power range.

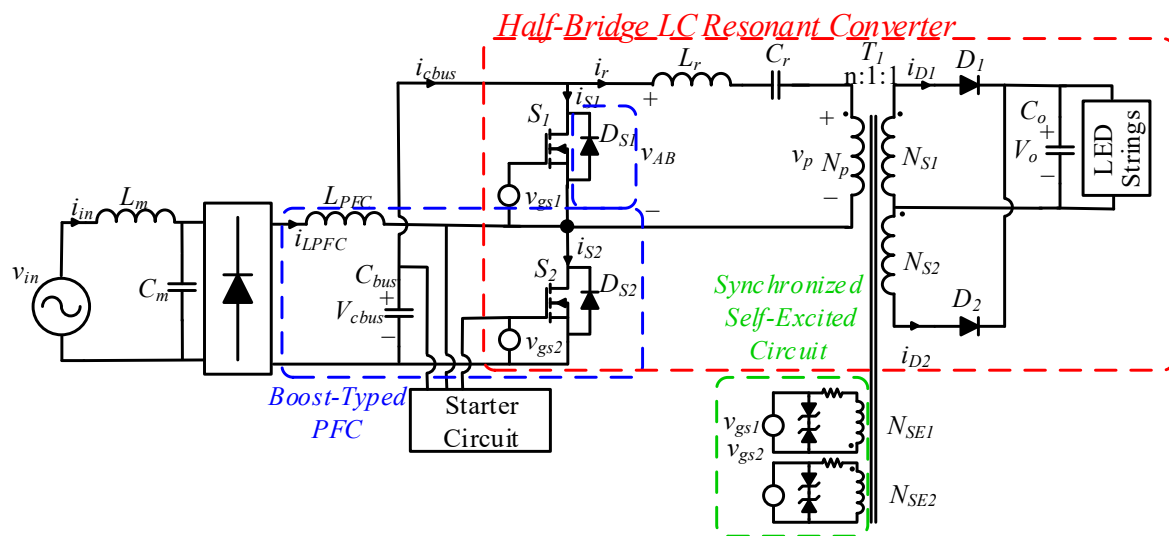


Figure 1. The developed, synchronized, self-excited, single-stage, high power-factor light-emitting diode (LED) driver.

2.1. Self-Excited Driving Voltages

The center-tapped transformer has two additional windings—the turn ratio of the primary winding to the additional windings is m : 1:1. The self-excited driving voltages were obtained by stepping down the high-frequency square wave via the transformer. A pair of symmetrical square wave voltages (v_{gs1} , v_{gs2}) were generated by the self-excited windings, as depicted in Figure 2. Their frequency f_s was in synchronism with the resonant frequency f_r which was created by the combination of resonant inductor L_r and resonant capacitor C_r , as can be expressed by Equations (1) and (2).

$$f_r = \frac{1}{2\pi\sqrt{L_r C_r}} \tag{1}$$

$$f_s = f_r \tag{2}$$

The voltage on the primary winding v_p of the transformer can be achieved by Equation (3),

$$v_p = DV_{cbus}M_{vr} \tag{3}$$

where M_{vr} is the voltage gain of the resonant circuit, and D is the duty ratio of the lower-arm power switch S_2 . The control voltages v_{gs1} and v_{gs2} may be approximated as square waves, equal to:

$$v_{gs1} = -v_{gs2} = \frac{-v_p}{m} \tag{4}$$

where the negative sign indicates the phase relationship between v_{gs1} and v_{gs2} .

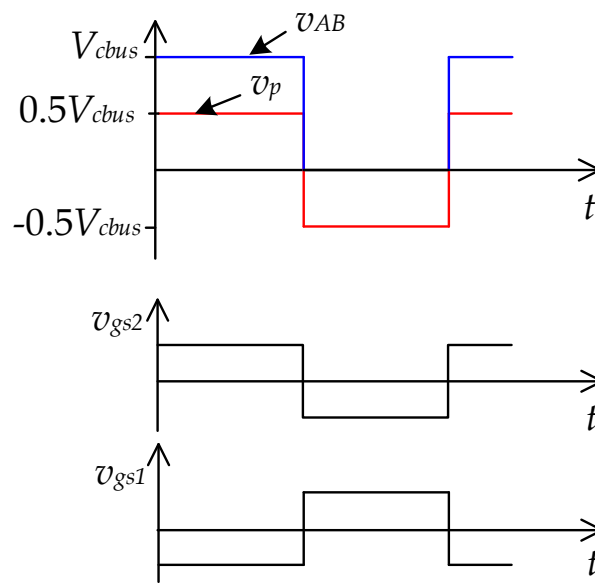


Figure 2. Schematic waveforms of the self-excited mechanism.

2.2. LC Resonant Converter

Since the self-excited driving voltages were directly obtained from the resonant circuit, the switching frequency of the power MOSFETs was, of course, synchronous with the resonant voltage waveform, thus making the switching frequency and the resonant frequency identical. The voltage gain M_{vr} of the resonant circuit is defined as the ratio of the magnitude of T_1 's primary voltage to the magnitude of the input voltage, and can be expressed as:

$$M_{vr} = \frac{V_p}{V_{AB}} = \frac{1}{\sqrt{1 + [Q(\frac{\omega_s}{\omega_r} - \frac{\omega_r}{\omega_s})]^2}} \tag{5}$$

$$Q = \frac{\sqrt{L_r/C_r}}{R_p} \tag{6}$$

where Q is the quality factor of the resonant circuit, ω_s designates the switching angular frequency, ω_r is the resonant angular frequency, and R_p represents the equivalent load resistance between the primary winding. At steady-state operation, R_p can be expressed as [22]:

$$R_p = \frac{8n^2 R_{LED}}{\pi^2} \tag{7}$$

where R_{LED} represents the equivalent impedance of the LED string. Figure 3 depicts the relationship between voltage gain M_{vr} and frequency ratio f_s/f_r based on Equations (5) and (6). It can be seen that the circuit exhibits capacitive characteristics when the switching frequency is smaller than the resonant frequency. The power switches will possess the feature of ZCS when $f_s/f_r < 1$. On the contrary, the circuit appears inductive when the switching frequency is greater than the resonant frequency. The power switches will possess ZVS when $f_s/f_r > 1$. As soon as the switching frequency and the resonant frequency are equal, the circuit possesses a resistive feature and the power switches can operate at both ZCS and ZVS. Figure 4 shows the ideally schematic waveforms of the input voltage of the resonant circuit v_{AB} and the resonant current i_r when $f_s = f_r$, i.e., that the voltage switches to zero the moment the resonant current reaches zero. This makes the power switch undergo no extra switching loss.

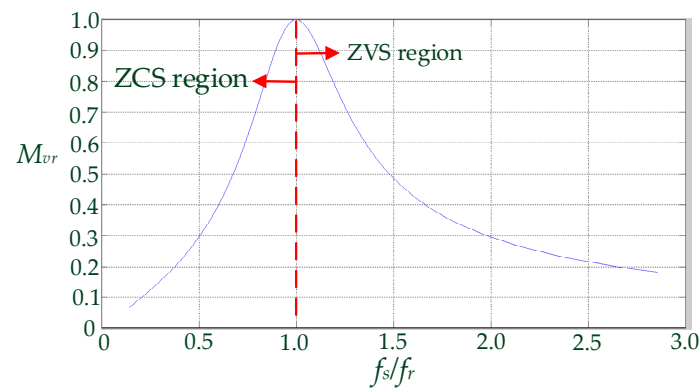


Figure 3. Voltage gain versus frequency ratio.

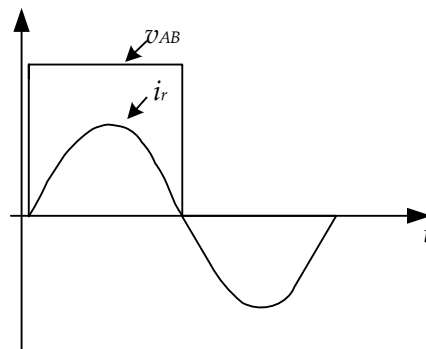


Figure 4. Voltage and current waveforms of the resonant circuit ($f_s = f_r$).

2.3. Boost-Typed Power-Factor Corrector

As shown in Figure 1, the boost converter, which is composed of L_{PFC} , S_2 , D_{S1} , and C_{bus} , performs the function of PFC. Figure 5 shows the PFC inductor current i_{LPFC} when the PFC circuit is designed to operate at discontinuous conduction mode (DCM). Since the rising slope of i_{LPFC} is proportional to the line voltage v_{in} , the envelope of i_{LPFC} would be sinusoidal. The alternating current (ac)/dc converter was supplied from the ac line voltage.

$$v_{in}(t) = V_m \sin(2\pi f_L t) \tag{8}$$

where f_L and V_m are the frequency and amplitude of the line voltage source, respectively. In practice, f_L is much lower than the switching frequency, f_s , of the active switches. It is reasonable to consider the rectified input voltage as a constant over a high-frequency cycle. Figure 6 shows i_{LPFC} in one

high-frequency cycle where t_{on} is the conduction time of switch S_2 and t_f represents the fall time of i_{LPFC} . The duty ratio D is defined as:

$$D = \frac{t_{on}}{T_s} \tag{9}$$

where T_s is the period of the switching frequency. At DCM operation, the peak value of the inductor current can be expressed as:

$$i_{PK}(t) = \frac{|V_m \sin(2\pi f_L t)| \cdot t_{on}}{L_{PFC}} = \frac{(V_{cbus} - V_m \sin(2\pi f_L t)) \cdot t_f(t)}{L_{PFC}} \tag{10}$$

From Equation (10), relationship between t_{on} and t_f can be described as Equation (11).

$$t_f(t) = \frac{V_m \sin(2\pi f_L t)}{V_{cbus} - V_m \sin(2\pi f_L t)} t_{on} \tag{11}$$

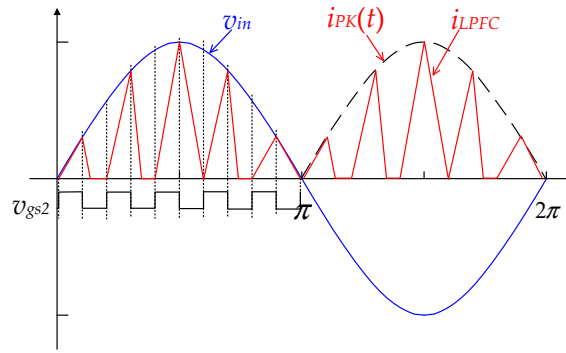


Figure 5. Schematic waveform of a power-factor corrector (PFC) inductor current.

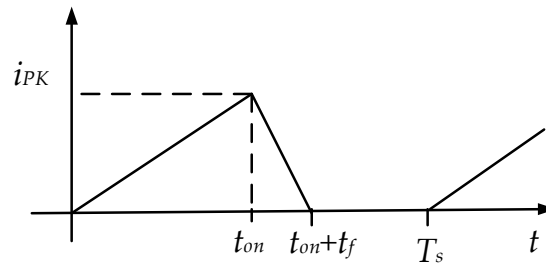


Figure 6. PFC inductor current in one high-frequency cycle.

The average value of i_{LPFC} over a high-frequency cycle is given, and can be expressed as [23]:

$$\overline{i_{LPFC}}(t) = \frac{(t_{on} + t_f(t)) \cdot i_{PK}(t)}{2T_s} = \frac{D^2 V_m |\sin(2\pi f_L t)|}{2L_{PFC} f_s} \cdot \frac{1}{1 - \frac{1}{k} \cdot |\sin(2\pi f_L t)|} \tag{12}$$

where the index k is defined as:

$$k \equiv \frac{V_{cbus}}{V_m} \tag{13}$$

The input current is equal to the average value of the PFC inductor current, and can be expressed as:

$$i_{in}(t) = \frac{D^2 V_m \sin(2\pi f_L t)}{2L_{PFC} f_s} \cdot \frac{1}{1 - \frac{1}{k} \cdot |\sin(2\pi f_L t)|} \tag{14}$$

The input power can be obtained by taking the average of the product of the input voltage and current over one line-frequency cycle. From Equations (8) and (14), the input power can be derived as [24]:

$$P_{in} = \frac{1}{\pi} \int_0^\pi V_m \sin(2\pi f_L t) \cdot i_{in}(t) d(2\pi f_L t) = \frac{D^2 V_m^2}{2L_{PFC} f_s} \cdot y \tag{15}$$

where y is expressed as:

$$y = \int_0^\pi \frac{\sin^2 \theta}{1 - \frac{1}{k} \sin \theta} d\theta = \frac{k^3}{\sqrt{k^2 - 1}} \left(1 + \frac{2}{\pi} \sin^{-1} \frac{1}{k} \right) - k^2 - \frac{2}{\pi} \cdot k \tag{16}$$

From Equations (15) and (16), the inductance of L_{PFC} can be calculated by using Equation (17).

$$L_{PFC} = \frac{\eta D^2 V_m^2}{2P_o f_s} \cdot y \tag{17}$$

where P_o and η represent the output power and circuit efficiency, respectively.

2.4. Starter Circuit

In the self-excited circuit, a circuit starter is indispensable to initialize the operation. Figure 7 shows the starter circuit used in the developed LED drive. The starter circuit is connected in parallel with the dc-bus capacitor C_{bus} with a simple resistor-capacitor (RC) circuit. Prior to the action of the starter, the dc-bus voltage V_{Cbus} charges toward C_{start} via R_{start} . With the time constant being represented by Equation (18), when the exponentially increasing voltage on the starting capacitor C_{start} reaches the breakover voltage of DIAC, the DIAC conducts and the power switch is triggered. As soon as S_2 commences to conduct, the resonant process begins. However, to avoid V_{Cbus} continually charging C_{start} , a bypass diode, D_{bp} , is connected across the power switch, S_2 . Of course, the bypass current through D_{bp} is drastically quantitatively smaller than the resonant current. To prevent the upper and lower switches from shooting through, the switching frequency needs to be far greater than the reciprocal of the time constant, as shown in Equation (19).

$$\tau = R_{start} C_{start} \tag{18}$$

$$f_s \gg \frac{1}{\tau} \tag{19}$$

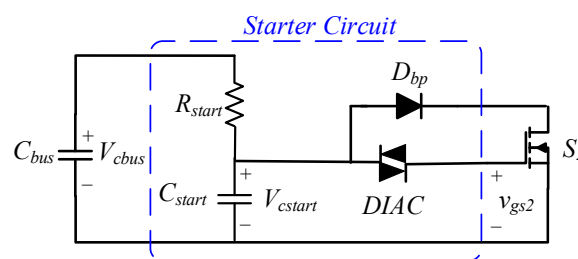


Figure 7. Starter circuit.

3. Circuit Analysis and Operation Modes

Figure 8 illustrates the schematic voltage and current waveforms of some key components. It can be inspected that both the PFC inductor current, i_{LPFC} , and the resonant current, i_r , flow through the power switch S_2 . When the input square voltage crosses zero, the resonant current becomes zero as well.

The input voltage of the resonant circuit is a square wave, and can be described by the Fourier expansion.

$$v_{AB}(t) = \sum_n \left[\frac{2V_{cbus}}{n\pi} \sin(2n\pi f_s t) \right] \quad n = 1, 3, 5 \dots \quad (20)$$

When the quality factor of the resonant circuit is high enough, almost all the harmonic contents of v_{AB} will be filtered out by the resonant circuit. Only the fundamental current at the switching frequency is present in the load resonant converter [22]. At steady-state operation, the voltage across the secondary winding is equal to the output voltage, and the load (including the output capacitance C_o) is fed by a rectified sinusoidal current source. The impedance across the secondary winding is equal to the resistance of the LED string (R_{LED}). Figure 9 shows the equivalent circuit of the resonant circuit, where v_1 represents the fundamental voltage of v_{AB} . From Equation (20), the root-mean-square (rms) value of the fundamental voltage is equal to:

$$V_1 = \frac{\sqrt{2}V_{cbus}}{\pi} \quad (21)$$

The impedance of the resonant circuit can be expressed as:

$$Z_{AB} = R_p + j \left(2\pi f_s L_r - \frac{1}{2\pi f_s C_r} \right) \quad (22)$$

Under this circumstance, the resonant current is sinusoidal, and can be expressed as:

$$i_r(t) = \frac{2V_{cbus}}{\pi Z_{AB}} \sin(2\pi f_s t) \quad (23)$$

From Equation (23), the resonant current would theoretically be zero in the case of failure and the load would go open circuit. However, in practical terms, a small current is there if the mutual inductance of the transformer is considered. On the contrary, in the case of failure where the load goes short circuit, the primary winding and the excited windings will all become short-circuited. Thus, both power switches will not be energized and the circuit will remain turned off. Besides, the LED current is not regulated in the proposed circuit since a self-excited control mechanism is used.

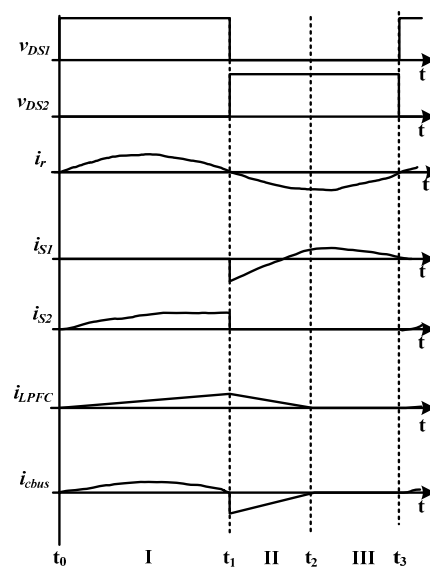


Figure 8. Schematic voltage and current waveforms of some key components.

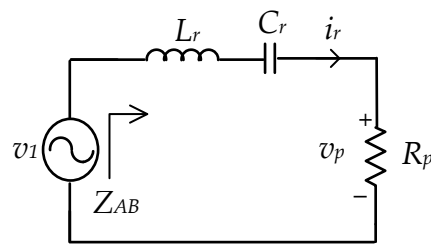


Figure 9. Equivalent circuit to the load resonant circuit.

At a steady state, the circuit operation can be divided into three modes in every high-frequency cycle. The current loops of each operation mode are shown in Figure 10, where v_{rec} represents the rectified voltage of the input line. As soon as the lower-arm power switch S_2 starts successfully, the circuit operation initiates. The operating modes are described below.

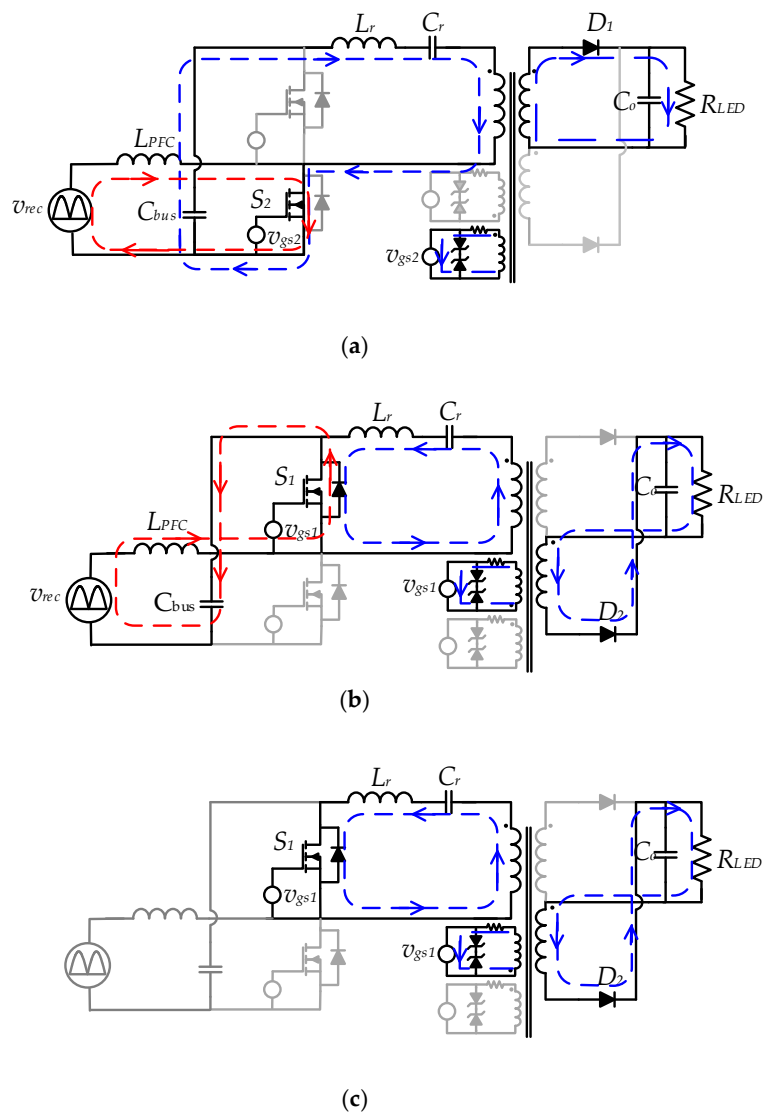


Figure 10. Equivalent circuit in different operation modes: (a) Mode I, (b) Mode II, and (c) Mode III.

3.1. Operation Mode I ($t_0 - t_1$)

In this mode, S_2 conducts, S_1 is off, and the rectified input voltage v_{rec} is across the boost inductor L_{PFC} . The PFC current i_{LPFC} flows through S_2 and increases linearly, as written in Equation (24).

$$i_{LPFC}(t) = \frac{V_m |\sin(2\pi f_L t)|}{L_{PFC}} (t - t_0) \quad (24)$$

In addition, the dc-bus voltage V_{cbus} is across the input of the resonant circuit and supplies a nearly sinusoidal resonant current, i_r . The i_r is positive and energizes the center-tapped transformer, as indicated in Figure 10a.

3.2. Operation Mode II ($t_1 - t_2$)

The equivalent circuit of Mode II is shown in Figure 10b. This mode starts as soon as the resonant current, i_r (via the center-tapped transformer) decreases to zero, and the primary winding then induces a back electromotive force (emf) and result in the conduction of power switch S_1 , along with the turn-off of switch S_2 . The current i_{LPFC} reaches a peak value at the beginning of Mode II. Since S_2 is off, the current i_{LPFC} diverts from S_2 to D_{S1} to charge the dc-bus capacitor C_{bus} . The voltage across L_{PFC} is equal to V_{cbus} minus v_{rec} , which is negative, meaning that i_{LPFC} decreases linearly.

$$i_{LPFC}(t) = \frac{V_m |\sin(2\pi f_L t)| DT_s}{L_{PFC}} - \frac{V_{cbus} - V_m |\sin(2\pi f_L t)|}{L_{PFC}} (t - t_1) \quad (25)$$

In this mode the current i_r is negative. Simultaneously, the resonant tank releases energy to the load.

3.3. Operation Mode III ($t_2 - t_3$)

The equivalent circuit of Mode III is shown in Figure 10c. This mode starts when the current i_{LPFC} decreases to zero. In this mode, S_1 keeps conducting. The resonant current continually supplies energy via the center-tapped transformer to the output.

4. Circuit Implementation

Based on the above-mentioned circuit analysis and mathematical derivations, a 40 W, 110 V_{ac}/95 V_{dc} half-bridge, self-excited, single-stage LED driver was implemented and realized. Table 1 outlines the circuit specification. The design criteria are briefly described as follows.

1. The PFC current i_{LPFC} is designed to operate in boundary conduction mode (BCM) when the input voltage gets near the peak value. By this way, the PFC converter would operate at DCM over the whole input line cycle.
2. By using this self-excited control mechanism, the duty ratio D of both MOSFETs is 0.5. The dc-bus voltage V_{cbus} should be sufficiently high to ensure the PFC converter operate at DCM. Theoretically, V_{cbus} should be higher than two times of the amplitude of the input line voltage at 0.5 duty ratio. In this illustrative example, V_{cbus} is designed to be 320 V.
3. Due to the self-excited mechanism, the driving voltages are fetched from the center-tapped transformer by means of the resonant current. The switching frequency is in synchronism with the resonant frequency. The resonant frequency is controlled by the selection of the resonant inductor and the resonant capacitor as is designed with 36 k Hz resonant frequency. The higher resonant frequency will detrimental to self-excited signal response. It will increase the rise and fall times of switching current, thus leading to extra switching loss.
4. Following determination of the resonant frequency f_r , only one single resonant capacitor is used with capacitance 10 nF. Accordingly, the resonant inductance can be achieved by Equation (1).

5. Substituting input voltage V_{in} , dc-bus voltage V_{Cbus} and switching frequency f_s into Equations (13), (16) and (17), the PFC inductor L_{PFC} can be obtained by the aid of numerical computation.
6. Since all the transferred power goes through the resonant capacitor, it is suggested to use a capacitor with low equivalent series resistance (ESR).

Table 1. Circuit Specification.

Input Voltage v_{in}	110 V _{rms} , 60 Hz
DC-bus voltage V_{cbus}	320 V _{dc}
Output voltage V_o	95 V
Output Current I_o	0.42 A
Switching frequency f_s	36 kHz

5. Experimental Results

A prototype circuit was built and tested. The circuit parameters are shown in Table 2, and the prototype circuit is shown in Figure 11. The experimental apparatuses consisted of an oscilloscope (Lecroy HDO4034, New York, NY, USA), voltage probes (Cybertek DP6150A, Shenzhen, China), current probes (Cybertek CP8030A, Shenzhen, China), and a power quality analyzer (Precision International Corp. PA-750B, New Taipei City, Taiwan). Figure 12 shows the measured voltage waveform on the primary winding and the self-excited windings of the center-tapped transformer. It can be seen that the self-excited voltage v_{gs1} and v_{gs2} are in phase with the primary voltage v_p . Obviously, the driving voltages v_{gs1} and v_{gs2} are symmetrically displaced by 180°. Hence, the switching frequency of the power switch could be the same as the resonant frequency of the resonant converter. Figure 13 shows the input voltage of the resonant converter v_{AB} and the resonant current i_r . It demonstrates that i_r is in phase with v_{AB} . This marks the equality of the resonant frequency and switching frequency, i.e., $f_r = f_s$.

Table 2. Circuit parameters.

Low-Pass Inductor L_m	1.8 mH
Low-pass capacitor C_m	0.47 μ F
DC-bus capacitor C_{bus}	100 μ F
Output capacitor C_o	50 μ F
Boost inductor L_{PFC}	1.3 mH
Resonant inductor L_r	1.8 mH
Resonant capacitor C_r	10 nF
Turns of the center-tapped transformer	$N_p = 64$ turns, $N_{S1} = N_{S2} = 40$ turns $N_{SE1} = N_{SE2} = 6$ turns
Power Switches S_1, S_2	IRF840

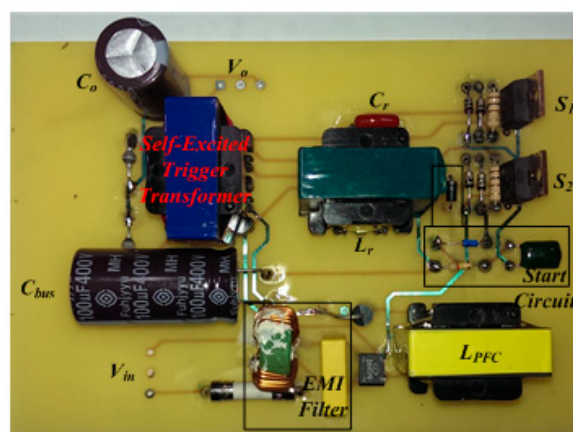


Figure 11. Prototype Circuit.

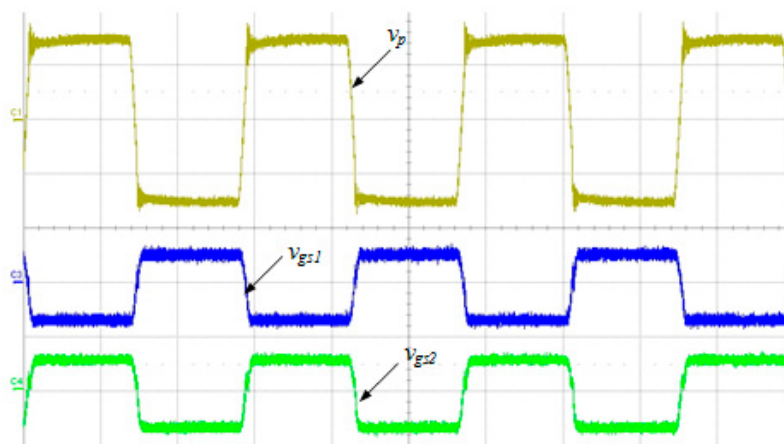


Figure 12. Voltage waveforms of the center-tapped transform. (v_p : 100 V/div, v_{gs1} , v_{gs2} : 20 V/div, time: 10 μ s/div).

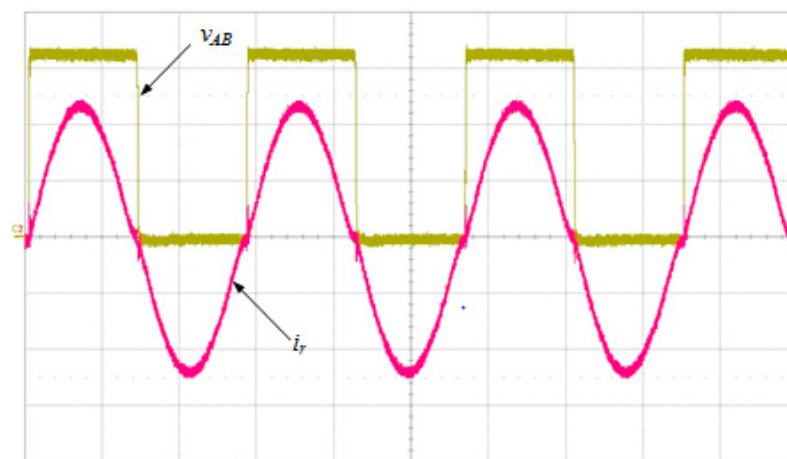


Figure 13. Voltage and current waveforms of the resonant converter. (v_{AB} : 100 V/div, i_r : 0.2 A/div, time: 10 μ s/div).

Figure 14 shows the waveforms of the input line voltage and the PFC inductor current i_{LPFC} . It reveals that the envelope of i_{LPFC} is in phase with the low-frequency input line voltage. Figure 15 shows the waveforms of i_{LPFC} and the voltage across the power switch S_2 . It indicates that the PFC converter operates at BCM when the input line voltage is at the peak value, while it operates at DCM elsewhere. The waveforms of the input line voltage and current are shown in Figure 16. It can be seen that the input current is in phase with the line voltage. The measured unity power factor and total current harmonic distortion (THDi) is 0.98 and 10.2%, respectively. It is seen that the input current is close to a triangle waveform. In this proposed circuit, the power switches are operated at a fixed switching frequency and fixed duty ratio ($D = 0.5$). Since the boost-typed PFC operates at DCM, the peak value of the inductor current is proportional to the rectified input voltage, i.e., the envelope of the inductor current would be a sinusoidal waveform. Theoretically, the average value of the rising portion of the inductor current within a high-frequency cycle is also sinusoidal. Nevertheless, the duration of the inductor current dropping from peak to zero is not constant. The higher the input voltage, the longer the declining duration. When the PFC operates at the time when the input voltage is at the peak of a sinusoidal waveform, the average value of the inductor current would be much higher than the peak. This is why the current waveform looks triangular.

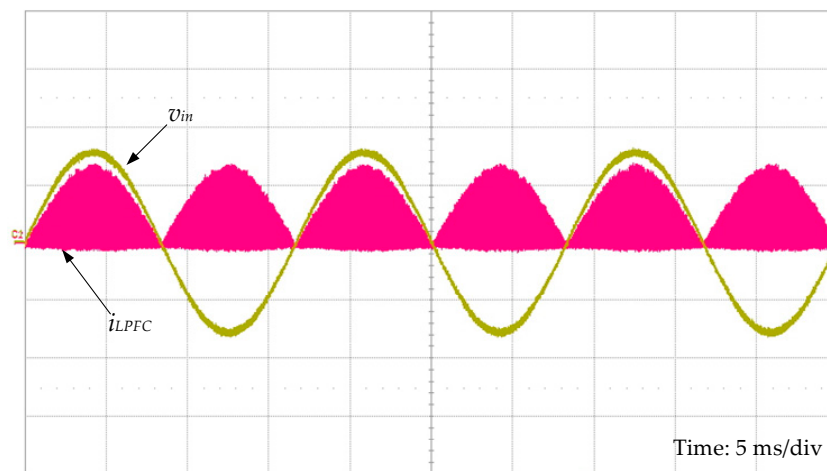
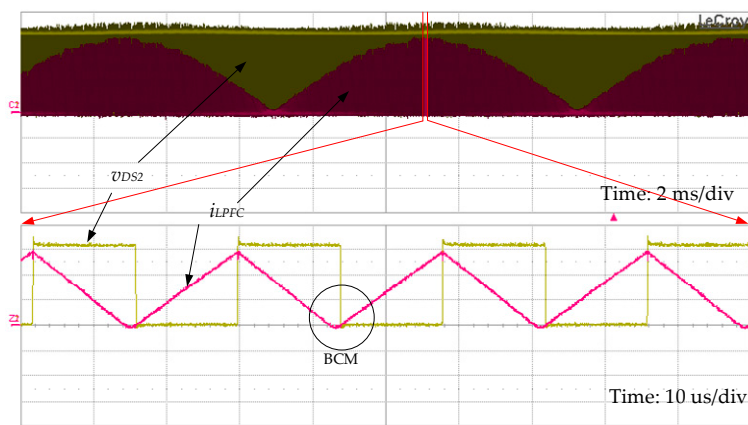
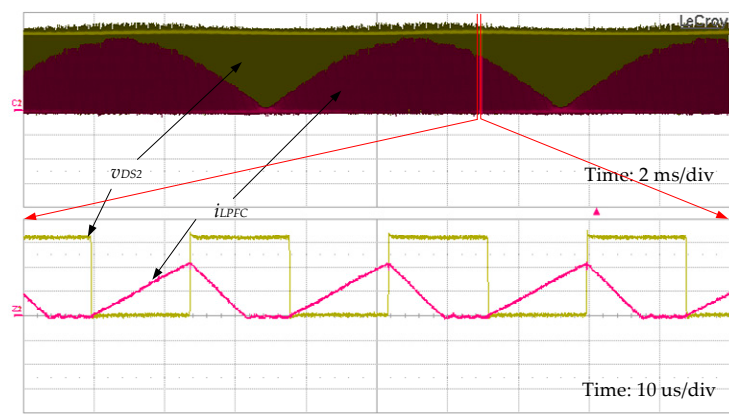


Figure 14. Waveforms of the input voltage and the PFC inductor current. (v_{in} : 100 V/div, i_{LPFC} : 1.0 A/div, time: 5 ms/div).



(a)



(b)

Figure 15. Waveforms of the PFC inductor current and the voltage across S_2 at (a) the peak value, and (b) near 135 degrees of the input line voltage. (v_{DS2} : 100 V/div, i_{LPFC} : 0.5 A/div).

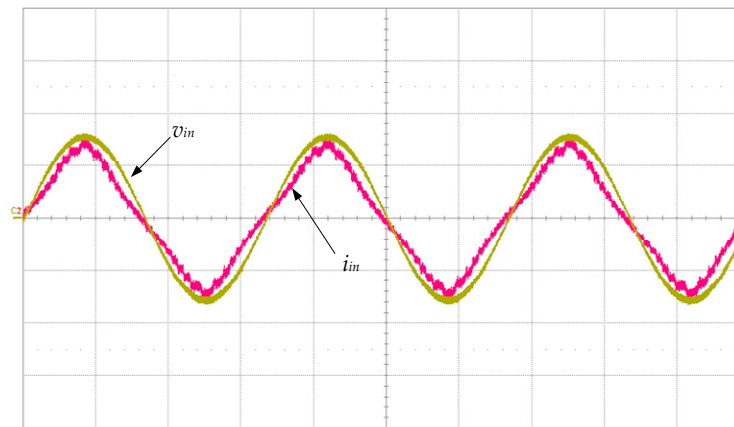


Figure 16. Waveforms of the input line voltage and current. (v_{in} : 100 V/div, i_{in} : 0.5 A/div, time: 5 ms/div).

Figure 17 shows the voltage and current waveforms of the power switches. Since the switching frequency is identical to the resonant frequency, S_1 can be turned off at zero current. Besides, as mentioned in operation Mode II, the PFC inductor current diverts from S_2 to D_{S1} as soon as S_2 is turned off. In this way, the voltage across S_1 is clamped to near zero volts. It helps the power switch S_1 to be turned on at zero voltage. Theoretically, the power switch S_2 should be turned on at zero voltage when the resonant circuit presents a resistive characteristic. Nevertheless, it is shown that a spike current happens when S_2 is turned on, meaning that S_2 does not achieve ZVS operation.

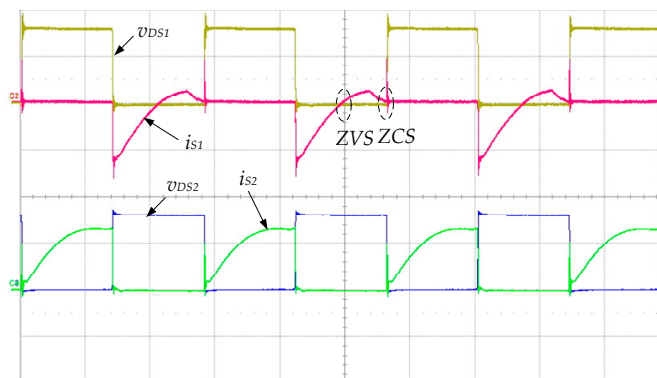


Figure 17. Voltage and current waveforms of the power switches. (v_{DS1} , v_{DS2} : 200 V/div, i_{S1} , i_{S2} : 1.0 A/div, time: 10 μ s/div).

At the output side of the developed circuit, the ZCS performance has been accomplished by inspecting the relationship between diode voltage waveforms and diode current waveforms on both D_1 and D_2 . Figure 18 obviously shows that the current of the output diodes naturally fall to zeros prior to the moment that the transformer secondary windings switch. It means that diodes D_1 and D_2 can operate at ZCS, resulting in a zero-recovery current and low turning-off losses. Figure 19 shows the waveforms of the output voltage and current, and as displayed, there are both high-frequency and low-frequency ripple components in the voltage and current. The measured average voltage and average current are 95 V and 0.42 A, respectively. The circuit efficiency is 92.2%. The measured values are consistent with the theoretical prediction, and the peak-to-peak voltage ripple is 560 mV, while the peak-to-peak current ripple is 46 mA. The ripple factors of the voltage and current are 0.6% and 10.9%, respectively.

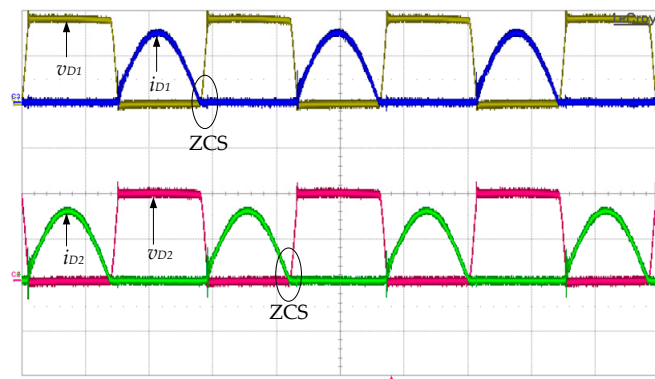


Figure 18. Voltage and current waveforms of the output diodes. (v_{D1} , v_{D2} : 100 V/div, i_{D1} , i_{D2} : 0.5 A/div, time: 10 μ s/div).

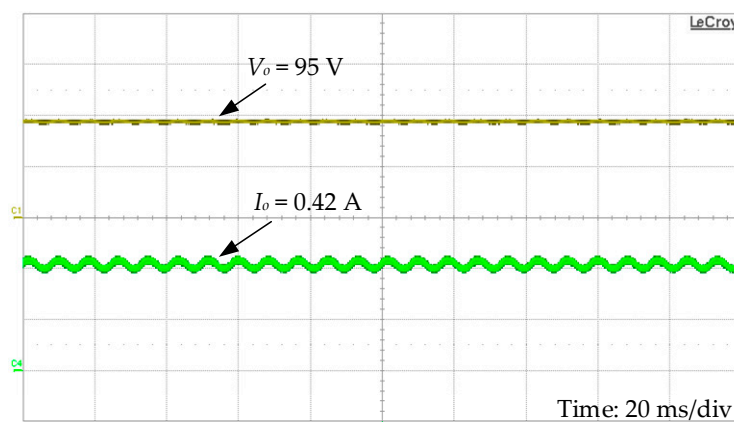


Figure 19. Waveforms of the output voltage and current. (v_{AB} : 50 V/div, i_r : 0.2 A/div, time: 20 ms/div).

6. Conclusions

In this research, a synchronized, self-excited control for a single-stage LED driver has been developed. The proposed circuit topology was derived by integrating a boost converter which functioned as a PFC, as well as a series resonant converter outputting a dc voltage to drive an LED string, which helps to save the number of power switches and their corresponding control circuits. In using this novel, self-excited driving approach, the proposed circuit does not need to use an integrated circuit. In addition, the components used to build a dc voltage for an integrated circuit could be saved. Because the driving voltages of the power switches are synchronized with the resonant current of the resonant circuit, the switching frequency and resonant frequency are identical, meaning that the power switch of the upper arm can operate at both ZVS and ZCS. However, the power switch of the lower arm cannot operate at ZCS, since it is shared by the PFC converter to help both the PFC inductor current and the resonant current to flow. Besides, the rectifying diodes at the output side possess the zero current cut-off characteristics. The high power factor and low THDi allow, by design, the boost-typed PFC converter to operate at DCM. The measured power factor and THDi are 0.98 and 10.2%, respectively, and the overall performance efficiency is 92.2%.

Author Contributions: Y.-N.C. conceived and designed the circuit; H.-L.C. performed circuit simulations and designed parameters of the circuit components; S.-Y.C. wrote the paper and H.-L.C. revised it for submission.

Funding: The research received no external funding.

Acknowledgments: This work was supported by the Ministry of Science and Technology, R.O.C. under Grant MOST 104-2622-E-150-005-CC3.

Conflicts of Interest: The authors declare no conflict of interest.

References

1. Gago-Calderón, A.; Hermoso-Orzáez, M.J.; De Andres-Diaz, J.R.; Redrado-Salvatierra, G. Evaluation of uniformity and glare improvement with low energy efficiency losses in street lighting LED luminaires using laser-sintered polyamide-based diffuse covers. *Energies* **2018**, *11*, 816. [[CrossRef](#)]
2. Van Duijnhoven, J.; Aarts, M.P.J.; Rosemann, A.L.P.; Kort, H.S.M. Ambiguities regarding the relationship between office lighting and subjective alertness: An exploratory field study in a Dutch office landscape. *Build. Environ.* **2018**, *142*, 130–138. [[CrossRef](#)]
3. Leccese, F.; Vandelanotte, V.; Salvadori, G.; Rocca, M. Blue light hazard and risk group classification of 8 W LED tubes, replacing fluorescent tubes, through optical radiation measurements. *Sustainability* **2015**, *7*, 13454–13468. [[CrossRef](#)]
4. Cheng, C.A.; Chang, E.C.; Tseng, C.H.; Chung, T.Y. A single-stage LED tube lamp driver with power-factor corrections and soft switching for energy-saving indoor lighting applications. *Appl. Sci.* **2017**, *7*, 115. [[CrossRef](#)]
5. Rospi, G.; Cardinale, N.; Negro, E. Energy performance and economic feasibility study of historical building in the city of Matera, southern Italy. *Energies* **2017**, *10*, 2009. [[CrossRef](#)]
6. Fantozzi, F.; Leccese, F.; Salvadori, G.; Rocca, M.; Garofalo, M. LED lighting for indoor sports facilities: Can its use be considered as sustainable solution from a techno-economic standpoint? *Sustainability* **2016**, *8*, 618. [[CrossRef](#)]
7. Yang, Y.R.; Chen, C.L. Steady-State Analysis and simulation of a BJT self-oscillating ZVS-CV ballast driven by a saturable transformer. *IEEE Trans. Ind. Electron.* **1999**, *46*, 249–260. [[CrossRef](#)]
8. Chen, F.Y.; Liang, T.J.; Lin, R.L.; Member, S.; Chen, J.F. A novel self-oscillating, boost-derived dc–dc converter with load regulation. *IEEE Trans. Power Electron.* **2005**, *20*, 65–74. [[CrossRef](#)]
9. Efrén, F.G.; Mario, P.S.; Luis, G.V.V.; Juarez, M.A.; Leobardo, H.G. Analysis and design method for high-frequency self-oscillating electronic ballasts. *IEEE Trans. Ind. Appl.* **2011**, *47*, 2430–2436.
10. Chan, S.S.M.; Chung, H.S.H.; Hui, S.Y. Design and analysis of an IC-less self-oscillating series resonant inverter for dimmable electronic ballasts. *IEEE Trans. Power Electron.* **2005**, *20*, 1450–1458. [[CrossRef](#)]
11. Soeiro, T.B.; Mühlethaler, J.; Linnér, J.; Ranstad, P.; Kolar, J.W. Automated design of a high-power high-frequency LCC resonant converter for electrostatic precipitators. *IEEE Trans. Ind. Electron.* **2013**, *60*, 4805–4819. [[CrossRef](#)]
12. Li, Z.; Park, C.Y.; Kwon, J.M.; Kwon, B.H. High-power-factor single-stage LCC resonant inverter for liquid crystal display backlight. *IEEE Trans. Ind. Electron.* **2011**, *58*, 1008–1015. [[CrossRef](#)]
13. Amjad, M.; Salam, Z. Design and implementation of a high-frequency LC-based half-bridge resonant converter for dielectric barrier discharge ozone generator. *IET Power Electron.* **2014**, *7*, 2403–2411. [[CrossRef](#)]
14. Youssef, M.Z.; Jain, P.K. A novel single stage ac–dc self-oscillating series-parallel resonant converter. *IEEE Trans. Power Electron.* **2006**, *21*, 1735–1744. [[CrossRef](#)]
15. Martín, F.J.F.; Viejo, C.B.; Antón, J.C.Á.; García, M.A.P.; Secades, M.R.; Alonso, J.M. Analysis and design of a high power factor, single-stage electronic ballast for high-intensity discharge lamps. *IEEE Trans. Power Electron.* **2003**, *18*, 558–569. [[CrossRef](#)]
16. Chuang, Y.C.; Moo, C.S.; Chen, H.W.; Lin, T.F. A novel single-stage high-power-factor electronic ballast with boost topology for multiple fluorescent lamps. *IEEE Trans. Ind. Appl.* **2009**, *45*, 323–331. [[CrossRef](#)]
17. Chang, Y.N. Self-excited single-stage power factor correction driving circuit for LED lighting. *J. Nanomater.* **2014**, *2014*, 1–8. [[CrossRef](#)]
18. Everts, J.; Krismer, F.; Keybus, J.V.; Driesen, J.; Kolar, J.W. Optimal ZVS modulation of single-phase single-stage bidirectional DAB ac-dc converters. *IEEE Trans. Power Electron.* **2014**, *29*, 3954–3970. [[CrossRef](#)]
19. Mishima, T.; Takami, C.; Nakaoka, M. A new current phasor-controlled ZVS twin half-bridge high-frequency resonant inverter for induction heating. *IEEE Trans. Ind. Electron.* **2014**, *61*, 2531–2545. [[CrossRef](#)]
20. Guo, Y.; Li, S.; Lee, A.T.L.; Tan, S.C.; Lee, C.K.; Hui, S.Y.R. Single-stage ac/dc single-inductor multiple-output LED drivers. *IEEE Trans. Power Electron.* **2016**, *31*, 5837–5850. [[CrossRef](#)]
21. Wang, S.; Ruan, X.; Yao, K.; Tan, S.C.; Yang, Y.; Ye, Z. A flicker-free electrolytic capacitor-less ac–dc LED driver. *IEEE Trans. Power Electron.* **2012**, *27*, 4540–4548. [[CrossRef](#)]
22. Cheng, H.L.; Hsieh, Y.C.; Lin, C.S. A novel single-stage high-power-factor ac/dc converter featuring high circuit efficiency. *IEEE Trans. Ind. Electron.* **2011**, *58*, 524–532. [[CrossRef](#)]

23. Chang, C.H.; Cheng, C.A.; Chang, E.C.; Cheng, H.L.; Yang, B.E. An integrated high-power-factor converter with ZVS transition. *IEEE Trans. Power Electron.* **2016**, *31*, 2362–2371. [[CrossRef](#)]
24. Liu, K.H.; Lin, Y.L. Current waveform distortion in power factor correction circuits employing discontinuous-mode boost converters. In Proceedings of the 20th Annual IEEE Power Electronics Specialists Conference, Milwaukee, WI, USA, 26–29 June 1989; pp. 825–829.



© 2018 by the authors. Licensee MDPI, Basel, Switzerland. This article is an open access article distributed under the terms and conditions of the Creative Commons Attribution (CC BY) license (<http://creativecommons.org/licenses/by/4.0/>).